CrossMark

Studies on the luminescence behavior of $SrCaMgSi_2O_7:Eu^{3+}$ phosphor by solid state reaction method

Ishwar Prasad Sahu[1] · D. P. Bisen[1] · N. Brahme[1] · Raunak Kumar Tamrakar[2]

Abstract A new orange–red europium doped strontium calcium magnesium di-silicate ($SrCaMgSi_2O_7:Eu^{3+}$) phosphor was prepared by the traditional high temperature solid state reaction method. The tetragonal structure of the orange–red compound was confirmed by the X-ray diffraction (XRD) technique. An energy dispersive X-ray spectroscopy (EDS) confirms the presence of elements in sintered phosphor. The thermoluminescence (TL) kinetic parameters such as activation energy, order of kinetics and frequency factor was calculated by peak shape method. In this work, the orange–red emission originated from the $^5D_0$–^7F_J (J = 0, 1, 2, 3, 4) transitions of Eu^{3+} ions could clearly be observed after sample was excited at 396 nm. Commission International de I'Eclairage color chromaticity diagram, TL spectra and ML spectra confirms the prepare $SrCaMgSi_2O_7:Eu^{3+}$ phosphor exhibits orange–red emission. The mechanoluminescence (ML) intensity of $SrCaMgSi_2O_7:Eu^{3+}$ phosphor increases linearly with increasing impact velocity of the moving piston which suggests that this phosphor can be used as sensors to detect the stress of an object. Thus, the present investigation indicates the piezo-electricity was responsible to produce ML in prepared $SrCaMgSi_2O_7:Eu^{3+}$ phosphor.

✉ Ishwar Prasad Sahu
ishwarprasad1986@gmail.com

[1] School of Studies in Physics and Astrophysics, Pt. Ravishankar Shukla University, Raipur, C.G. 492010, India

[2] Department of Applied Physics, Bhilai Institute of Technology, Durg, C.G. 491001, India

1 Introduction

Rare earth oxides (RE_2O_3) are the most stable rare earth compounds, in which the rare earth ions hold typically a trivalent state [1]. Rare earth oxides have been widely used in the field of luminescent devices, optical transmission, bio-chemical probes, medical diagnosis and so for, because of their optical, electronic and chemical properties resulting from their 4f electrons [2, 3]. Inorganic compounds doped with trivalent europium cations (Eu^{3+}) are used for many different applications. The luminescence properties of Eu^{3+} ions involve intra $4f^6$ (4f–4f) transitions mechanisms between excited state to ground state [4, 5]. The emission wavelength of the 4f–4f transition of Eu^{3+} is relatively insensitive to the host and temperature because the 4f shell is shielded by the outer filled 5s and 5p shells. Eu^{3+} ions are employed in luminescent devices such as fluorescent lamps and cathode ray tubes [6]. Currently transitions of Eu^{3+} ions have attracted considerable interest owing to the attempt to develop novel phosphors that can improve the color temperatures and the color rendering index of White Light Emitting Diode (WLED) [7].

Melilite are a large group of compounds characterized by the general formula $M_2T^1T^2_2O_7$, (M = Sr, Ca, Ba; T^1 = Mn, Co, Cu, Mg, Zn; T_2 = Si, Ge), have been investigated widely as optical materials [8]. Recently strontium calcium magnesium di-silicate ($SrCaMgSi_2O_7$) phosphor has attracted great interest due to its special structure features, excellent physical and chemical stability [9, 10]. Due to their tetragonal and non-centrosymmetric crystal structure, lanthanides or transition metals can be accepted easily as constituents or dopants by the melilites, allowing the synthesis of high-quality doped single

crystals. Alkaline earth silicate is an important luminescent material because of its excellent chemical, thermal stabilization and cheap raw material (SiO_2) [11]. It is well known that Eu^{2+} activated alkaline earth silicate such as $Sr_2MgSi_2O_7:Eu^{2+}$; $Sr_2Al_2SiO_7:Eu^{2+}$; $Ca_2Al_2SiO_7:Eu^{2+}$ and $Ca_2MgSi_2O_7:Eu^{2+}$; $SrCaMgSi_2O_7:Eu^{2+}$ phosphors have also been largely investigated [12–15].

Most of the silicate based phosphors which possess the tetragonal and non-centrosymmetric crystal structure, also have the ability to produce ML. ML has found various important applications such as impact sensors in spacecrafts (the emission intensity can be used to determine the kinetic energy of impact), fracture sensor, damage sensor, stress sensor for the visualizations of stress field near the crack-tip, stress distribution in the solids, and quasidynamic crack-propagation in solids etc. Thus, many researchers have been focused on the investigation of phosphors with high ML [16, 17].
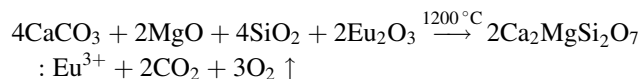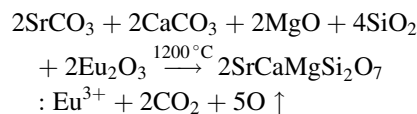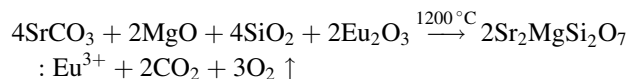
Recently, considerable efforts have been devoted to the research of new red or orange–red materials used for white LEDs. Quite a lot of luminescent materials activated by rare earth ions have been invented. So, we synthesized $SrCaMgSi_2O_7:Eu^{3+}$ phosphor and studied the luminescent properties. To the best of our knowledge, there is no report about the orange–red $SrCaMgSi_2O_7:Eu^{3+}$ phosphor for potential application on WLEDs and stress sensors. In this paper, we report the phosphor synthesis, structural characterization and luminescence properties of $SrCaMgSi_2O_7:Eu^{3+}$ phosphor by solid state reaction method. Investigation on the crystal structure, surface morphology, elemental analysis, different stretching band of sintered phosphor was determined by the X-ray diffraction (XRD), field emission scanning electron microscopy (FESEM), energy dispersive X-ray spectroscopy (EDS) and fourier transform infrared spectroscopy (FTIR) techniques. Luminescence properties were also investigated on the basis of TL, PL, decay, ML and ML spectra studies.

2 Experimental

2.1 Phosphor synthesis

Europium doped strontium calcium magnesium di-silicate namely $SrCaMgSi_2O_7:Eu^{3+}$ phosphor was prepared by the high temperature solid state reaction method. The raw material was strontium carbonate [$SrCO_3$ (99.90 %)], calcium carbonate [$CaCO_3$ (99.90 %)], magnesium oxide [MgO (99.90 %)], silicon di-oxide [SiO_2 (99.99 %)] and europium oxide [Eu_2O_3 (99.99 %)], all of analytical grade (A. R.), were employed in this experiment. Boric acid (H_3BO_3) was added as flux. The small amounts of flux,

improve the phosphor long afterglow luminescent intensity, reduce the phosphor synthetic temperature, improve the phosphor synthetic quality, and increase the production rate. The chemical reaction used for stoichiometric calculation is:

$$4SrCO_3 + 2MgO + 4SiO_2 + 2Eu_2O_3 \xrightarrow{1200\,°C} 2Sr_2MgSi_2O_7 : Eu^{3+} + 2CO_2 + 3O_2 \uparrow$$

$$2SrCO_3 + 2CaCO_3 + 2MgO + 4SiO_2 + 2Eu_2O_3 \xrightarrow{1200\,°C} 2SrCaMgSi_2O_7 : Eu^{3+} + 2CO_2 + 5O \uparrow$$

$$4CaCO_3 + 2MgO + 4SiO_2 + 2Eu_2O_3 \xrightarrow{1200\,°C} 2Ca_2MgSi_2O_7 : Eu^{3+} + 2CO_2 + 3O_2 \uparrow$$

Initially, raw materials were weighed according to the nominal compositions of $SrCaMgSi_2O_7:Eu^{3+}$ phosphor. Then the powders were mixed and milled thoroughly for 2 h using the mortar and pestle. The ground sample was placed in an alumina crucible and subsequently fired at 1200 °C for 3 h in an air. In order to investigate the crystal structure of the $SrCaMgSi_2O_7:Eu^{3+}$ phosphor, we also prepare $Sr_2MgSi_2O_7:Eu^{3+}$ and $Ca_2MgSi_2O_7:Eu^{3+}$ phosphors at same temperature. At last the nominal compounds were obtained after the cooling down of programmable furnace and products were finally ground into powder for characterizing the phosphors.

2.2 Measurement techniques

The crystal structure of the prepared $SrCaMgSi_2O_7:Eu^{3+}$ phosphor was characterized by powder XRD analysis. Powder XRD pattern has been obtained from Bruker D8 advanced X-ray powder diffractometer and the data were collected over the 2θ range 10°–80°. The X-rays were produced using a sealed tube (CuKα radiation source and the wavelength of X-ray was (1.54 Å). The X-rays were detected using a fast counting detector based on silicon strip technology (Bruker LynxEye detector). The crystal structure of the sample was verified with the help of Joint Committee of Powder Diffraction Standard Data (JCPDS) file. The morphological images of prepared phosphor were collected by the FESEM. The sample was coated with a thin layer of gold (Au) and then the surface morphology of prepared phosphor was observed by FESEM; ZIESS Ulta Plus-55 operated at the acceleration voltage of 5 kV. An EDS spectrum was used for the elemental (qualitative and quantitative) analysis of the prepared phosphor. FTIR spectra was recorded with the help of IR Prestige-21 by SHIMADZU for investigating the finger print region (1400–400 cm^{-1}) and functional groups (4000–1400 cm^{-1}) of prepared phosphor. The FTIR spectrum was collected in the middle infrared region

(4000–400 cm^{-1}) by mixing the potassium bromide (KBr, IR grade) with prepared SrCaMgSi$_2$O$_7$:Eu^{3+} phosphor. TL glow curve was recorded with the help of TLD reader 1009I by Nucleonix (Hyderabad, India Pvt. Ltd.). The excitation and emission spectrum was recorded on a Shimadzu (RF 5301-PC) spectrofluorophotometer using the Xenon lamp (150 W) as excitation source when measuring. The color chromaticity coordinates were obtained according to CIE 1931. The decay curves were obtained using a Perkin Elmer fluorescence spectrometer with the proper excitation under a UV lamp (365 nm). The ML measurement was observed by the home made lab system comprising of an RCA-931A photomultiplier tube (PMT). The ML glow curve can be plotted with the help of SM-340 application software installed in a computer attached with the storage oscilloscope. The TL and ML spectrum was recorded with the help of different band pass interference (400–700 nm) filters. All measurements were carried out at the room temperature.

3 Results and discussions

3.1 XRD analysis

In order to investigate the crystal structure, powder XRD analysis has been carried out. XRD patterns of SrCaMgSi$_2$O$_7$:Eu^{3+} phosphor with Sr$_2$MgSi$_2$O$_7$:Eu^{3+} and Ca$_2$MgSi$_2$O$_7$:Eu^{3+} phosphors were shown in Fig. 1a. The standard XRD patterns of SrCaMgSi$_2$O$_7$ was not found in the International Center for Diffraction Data (ICDD) database but compared with the standard patterns of Sr$_2$MgSi$_2$O$_7$ (JCPDS 75-1736) and Ca$_2$MgSi$_2$O$_7$ (JCPDS 77-1149) [18, 19], it could be seen that the major diffraction peaks of SrCaMgSi$_2$O$_7$:Eu^{3+} are similar for both alkaline earth silicates. The result reveals that the SrCaMgSi$_2$O$_7$:Eu^{3+} phosphor has the same crystal structure as Sr$_2$MgSi$_2$O$_7$ and Ca$_2$MgSi$_2$O$_7$ phosphors. In addition, the location of its diffraction peaks was between of the corresponding peaks of Sr$_2$MgSi$_2$O$_7$ and Ca$_2$MgSi$_2$O$_7$ phosphors, which indicates that the change of alkaline earth ions induces a small effect on the structure of the sample [20].

These results reveals that the crystal structure of Sr$_2$MgSi$_2$O$_7$:Eu^{3+}; SrCaMgSi$_2$O$_7$:Eu^{3+} and Ca$_2$MgSi$_2$O$_7$:Eu^{3+} phosphors has an akermanite type structure which belongs to the tetragonal crystallography with space group P$\overline{4}2_1$m, this structure was the member of the melilite group and forms layered compound [21]. Figure 1b shows the enlarged XRD patterns of Sr$_2$MgSi$_2$O$_7$:Eu^{3+}; SrCaMgSi$_2$O$_7$:Eu^{3+} and Ca$_2$MgSi$_2$O$_7$:Eu^{3+} phosphors on the (2 1 1) crystal planes, over the 2θ range 30.20°–31.60°. In
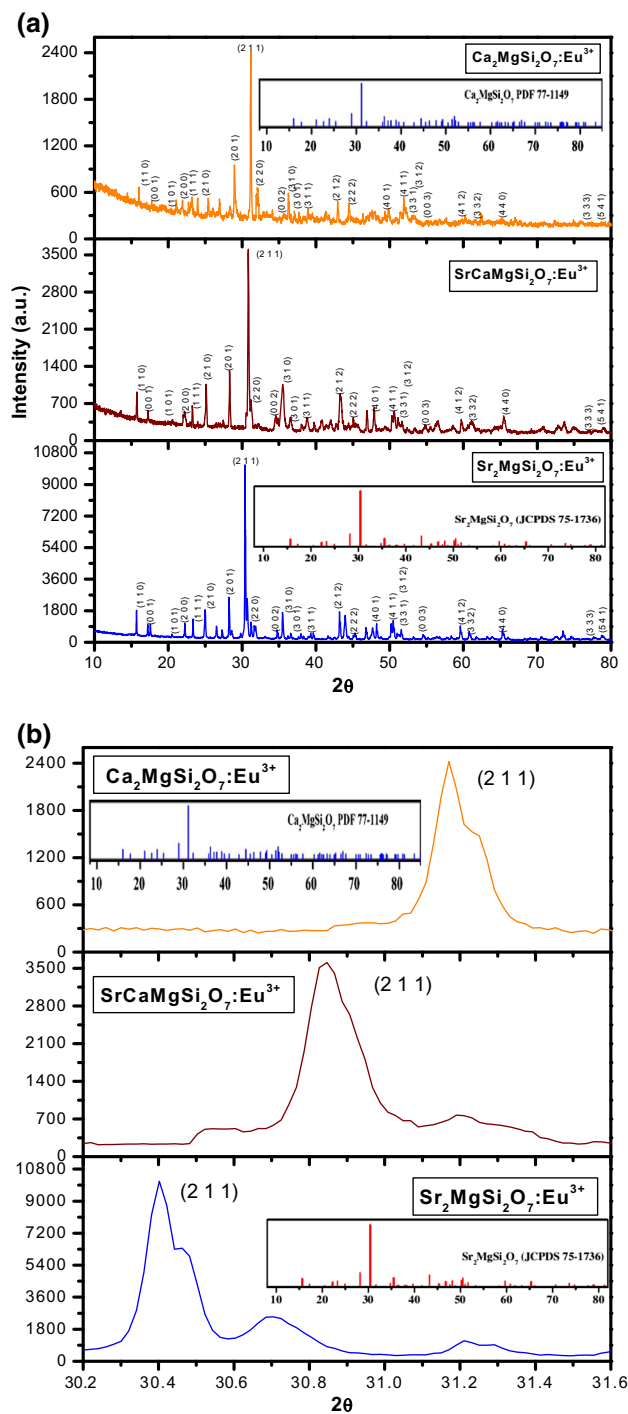
Fig. 1 **a** XRD patterns of Sr$_2$MgSi$_2$O$_7$:Eu^{3+}, SrCaMgSi$_2$O$_7$:Eu^{3+} and Ca$_2$MgSi$_2$O$_7$:Eu^{3+} phosphors. **b** Enlarged XRD patterns of Sr$_2$MgSi$_2$O$_7$:Eu^{3+}, SrCaMgSi$_2$O$_7$:Eu^{3+} and Ca$_2$MgSi$_2$O$_7$:Eu^{3+} phosphors for the (2 1 1) crystal planes

addition, the location of major diffraction peaks shifted towards higher angle compared with that of the corresponding peaks of Sr$_2$MgSi$_2$O$_7$:Eu^{3+} phosphor.

3.2 Field emission scanning electron microscopy (FESEM)

FESEM study was carried out to obtain information about surface morphology, grain size, and shape of the synthesized phosphor. The morphologies of prepared $SrCaMgSi_2O_7$:Eu^{3+} phosphor was also observed by means of FESEM in Fig. 2. The surface of the discussed $SrCaMgSi_2O_7$:Eu^{3+} phosphor has shown irregular shapes which means the distribution of the particle sizes was not homogeneous. From the FESEM image, it can be observed that the prepared phosphor consists of particles with different size distribution. The morphological images of prepared $SrCaMgSi_2O_7$:Eu^{3+} phosphor shows that the particles were aggregated tightly due to the high temperature synthesis technique.

3.3 Energy dispersive X-ray spectroscopy (EDS)

The chemical composition of the powder sample has been measured using an EDS spectrum. Figure 3 shows an EDS spectrum of $SrCaMgSi_2O_7$:Eu^{3+} phosphor. Table 1 shows the compositional elements of $SrCaMgSi_2O_7$:Eu^{3+} phosphor, which is compare with the standard element. The elements appear in ratios concomitant with the proportions mixed in the starting materials, which is representing the composition of the powder sample.

An EDS spectrum was a standard procedure for identifying and quantifying elemental (qualitative and quantitative) composition of sample area as small as a few nanometers. Their appeared no other emissions apart from strontium (Sr), calcium (Ca), magnesium (Mg), silicon (Si), oxygen (O) and europium (Eu) in $SrCaMgSi_2O_7$:Eu^{3+} phosphor in their corresponding EDS spectra. In the spectrum, intense peaks of compositional elements are

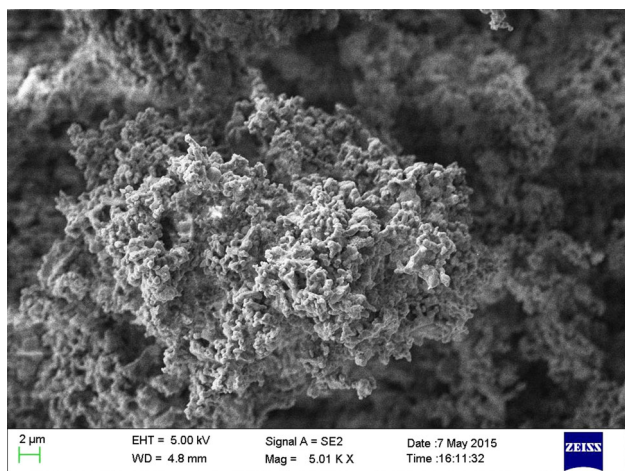**Fig. 3** EDS spectra of $SrCaMgSi_2O_7$:Eu^{3+} phosphor

Table 1 Composite element of $SrCaMgSi_2O_7$:Eu^{3+} phosphor

Sr. N.	Standard	Elements	Weight%	Atomic%
1	SiO_2	O K	23.40	42.28
2	MgO	Mg K	5.82	6.27
3	SiO_2	Si K	13.81	13.97
4	SrF_2	Sr L	28.88	19.32
5	Wollastonite	Ca L	26.85	17.07
6	EuF_3	Eu L	1.23	1.09
Total			100	100

present which confirm the presence of elements in $SrCaMgSi_2O_7$:Eu^{3+} phosphor.

3.4 Fourier transform infrared (FTIR) spectra

FTIR spectra have been widely used for the identification of organic and inorganic compounds. Figure 4 shows the FTIR spectra of $SrCaMgSi_2O_7$:Eu^{3+} phosphor. The appearance of the band related to the stretching vibrations of OH groups
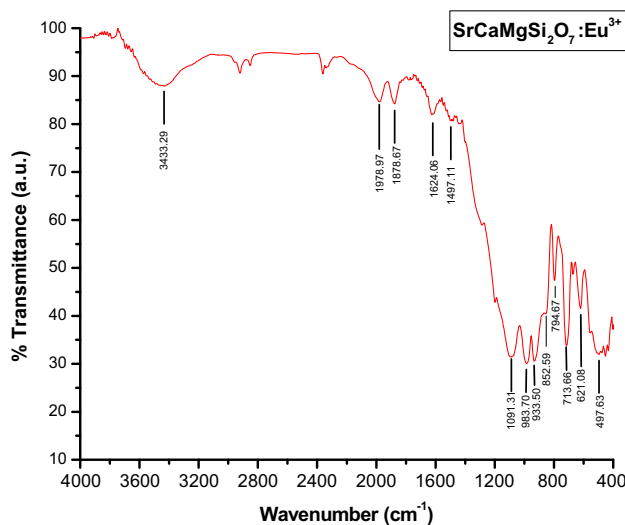

Fig. 2 FESEM micrograph of $SrCaMgSi_2O_7$:Eu^{3+} phosphor

Fig. 4 FTIR Spectra of $SrCaMgSi_2O_7$:Eu^{3+} phosphor

($\sim$3433.29 cm^{-1}) in the IR spectrum, is the evidence of hydration resulting from the absorption of atmospheric moisture. The asymmetric stretching of (CO_3^{2-}) carbonates can be observed $\sim$1978.97, 1878.67 cm^{-1}. These bands are due to a slight carbonation of the raw materials [$SrCO_3$ and $CaCO_3$]. The vibration band of $\sim$1624.06 cm^{-1} are assigned due to the Mg^{2+} and bending of the sharp peaks in the region of $\sim$1497.11 cm^{-1} are assigned due to the Sr^{2+} [22–24].

According to the crystal structure of $SrCaMgSi_2O_7$, the coordination number of strontium and calcium can be 8 and 6. Therefore, Sr^{2+} can occupy two alternative lattice sites, the eight coordinated site [SrO_8 (Sr_1 site)] and the six coordinated site [SrO_6 (Sr_2 site)], and other two independent cations sites, namely Mg^{2+} [MgO_4] and Si^{4+} [SiO_4] also exist in the crystal lattice. Mg^{2+} and Si^{4+} cations occupy the tetrahedral sites [25, 26]. Eu^{3+} ions can occupy two alternative lattice sites and the coordination number of europium can be can be 6, 8 and 9 [EuO_8 (Eu_1) and EuO_6 (Eu_2)]. It's hard for Eu^{3+} ions to incorporate the tetrahedral [MgO_4] or [SiO_4] symmetry but it can easily incorporate octahedral [SrO_8] or hexahedral [SrO_6]. Another fact that supports that the radius of Eu^{3+} (1.07 Å) are very close to that of Sr^{2+} (about 1.12 Å) and Ca^{2+} (about 1.12 Å) rather than Mg^{2+} (0.65 Å) and Si^{4+} (0.41 Å). Therefore, the Eu^{3+} ions are expected to occupy the Sr^{2+} and Ca^{2+} sites in the $SrCaMgSi_2O_7$:Eu^{3+} phosphor. The two peaks in the finger print region $\sim$852.59, 794.67 cm^{-1} are assigned due to the Ca^{2+} ions [27].

In the presented spectrum the absorption bands of silicate groups were clearly evident. According to previous studies on silicate materials, the position of the bands in the 1100–800 cm^{-1} region can provide information about the number of bridging oxygen atoms, bonded to silicon atoms. The intense band $\sim$1091.31, 983.70, 933.50 cm^{-1} was assigned to the Si–O–Si asymmetric stretch and Si–O symmetric stretch. The bands $\sim$713.66, 621.08 cm^{-1} are due to the Si–O–Si vibrational mode. The vibration band around $\sim$497.63 cm^{-1} is assigned due to the Mg^{2+}, which is based on the Mg–O modes. The groups [Si_2O_7] constitute diorthosilicates, are the main structural elements of melilites; which is presented in the discussed FTIR spectra of $SrCaMgSi_2O_7$:Eu^{3+} phosphor [28, 29].

3.5 Thermoluminescence (TL)

TL is the discharge of stored energy by thermal stimulation in the form of light. TL is observed under three conditions [30]. Phosphor irradiated with α-rays, β-rays, γ-rays, X-rays, UV rays etc. emits TL with a luminance that is nearly proportional to the luminance of the applied radiation. The relevant mechanism is as follows: the α-rays, β-rays, γ-rays, X-rays, UV rays excite the electrons of the

rare earth ions in the phosphor. Some of these excited electrons are captured by defects in the lattice. The electrons return to the ground state on thermal stimulation and the energy difference is emitted in the form of light [31].

In order to study the trap states of the prepared $SrCaMgSi_2O_7$:Eu^{3+} phosphor, TL glow curves were recorded and are shown in Fig. 5. The phosphor was first irradiated for 10 min using 365 nm UV source, then the radiation source was removed and the irradiated sample was heated at a linear heating rate of 5 °C/s, from room temperatures to 300 °C. Initially the TL intensity increases with temperature, attains a peak value for a particular temperature, and then it decreases with further increase in temperature. A single glow peak of $SrCaMgSi_2O_7$:Eu^{3+} phosphor was obtained at 192.7 °C, indicating that the electron traps involved are deep enough and high energy was required to release the trapped electrons; hence long storage of trapped charge carriers at normal working temperature was achieved and thus the thermal stability was ensured. The single isolated peak due to the formation of only one type of luminescence center which was created due to the UV irradiation. It is suggested that the recombination center associated with the glow at the temperature interval arises from the presence of liberated pairs, which are probably the results from the thermal release of electron/holes from electron/hole trap level and recombine at the color centers. It is also known that the doping of the rare earth ions increases the lattice defects which have existed already in the host. The TL kinetic parameters were calculated and listed in Table 2.
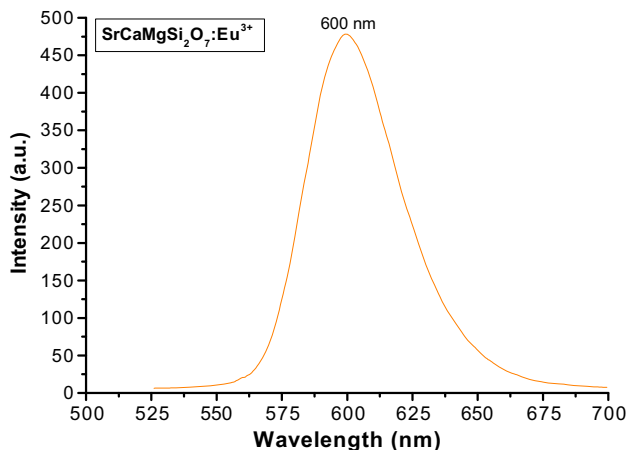
Figure 6 shows the TL emission spectra of $SrCaMgSi_2O_7$:Eu^{3+} phosphor. TL emission spectra of $SrCaMgSi_2O_7$:Eu^{3+} phosphor shows broad peak around 600 nm corresponds to orange–red color in the visible region. From, TL emission
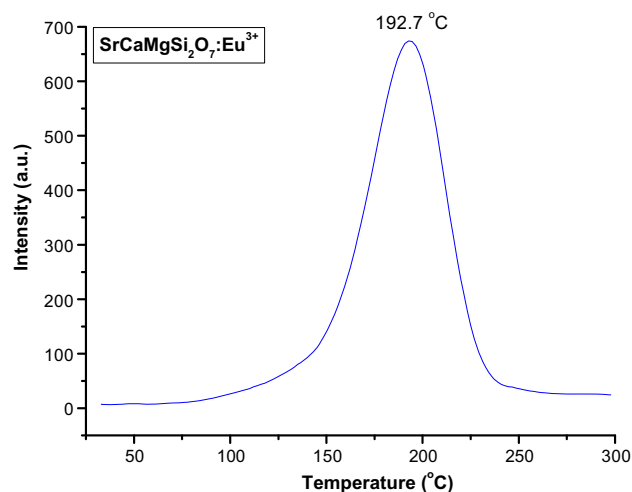
Fig. 5 TL glow curve of $SrCaMgSi_2O_7$:Eu^{3+} phosphor for 10 min UV irradiation

Table 2 Activation energy (E), frequency factor (s^{-1}) and shape factor (μ_g) for UV irradiated $SrCaMgSi_2O_7$:Eu^{3+} phosphor

UV min	HTR	T_1 (°C)	T_m (°C)	T_2 (°C)	τ (°C)	δ (°C)	ω (°C)	$\mu_g = \delta/\omega$	Activation energy (eV)	Frequency factor
10	5	167.98	192.7	214.90	24.72	22.20	46.92	0.47	1.32	9.5×10^{13}

Fig. 6 TL spectra of $SrCaMgSi_2O_7$:Eu^{3+} phosphor

Fig. 7 Schematic diagram of glow curve peak shape method

spectra of $SrCaMgSi_2O_7$:Eu^{3+} phosphor confirms the single isolated peak due to the formation of only one type of luminescence center which was created due to the UV irradiation.

3.6 Determination of kinetic parameters

The TL emission characteristic of a phosphor material mainly depends on the kinetic parameters describing the trapping-emitting centers which are quantitatively responsible. For example, the estimation of the time elapsed since exposure is closely related to the position of the trapping levels (E) within the band gap and frequency factor (s) of the electrons in the traps and therefore it is necessary to have a good knowledge of these parameters. There are various methods for evaluating the trapping parameters from TL glow curves [32].

Evaluation of kinetic parameters, associated with the glow peaks of the thermally stimulated luminescence, is one of the most studied subjects in the field of condensed matter physics and a complete description of the thermoluminescent characteristics of a TL material requires obtaining these parameters. There are various methods for evaluating the trapping parameters from TL glow curves. For example, when one of the TL glow peaks is highly isolated from the others, the experimental method such as peak shape method is a suitable method to determine kinetic parameters. The TL parameters for the prominent glow peaks of prepared phosphor were calculated using the peak shape method [33].
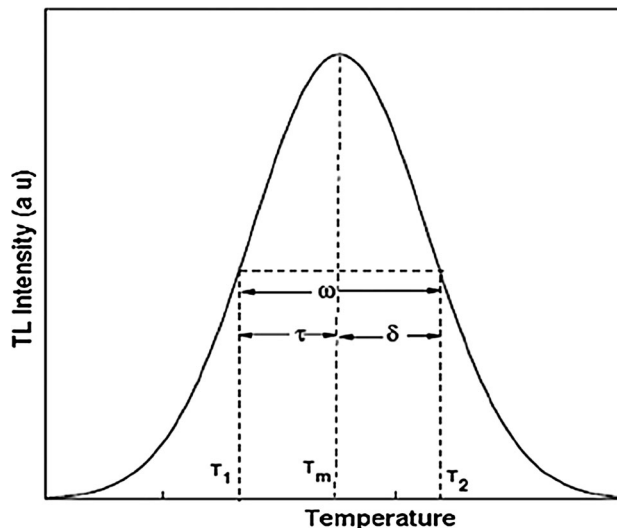
3.6.1 Glow curve peak shape method

Using the glow curve peak shape method the different shape parameters of the present $SrCaMgSi_2O_7$:Eu^{3+} phosphor namely the total half intensity $\omega = T_2 - T_1(\tau + \delta)$, τ is the half width at the low temperature side of the peak or the low temperature half width ($\tau = T_m - T_1$); δ is the half width towards the fall-off side of the glow peak or the high temperature half width ($\delta = T_2 - T_m$), and T_m is the peak temperature and T_1 and T_2 are temperature on either side of T_m corresponding to half peak intensity were determined and presented in Table 2. Figure 7 shows the schematic diagram of glow curve peak shape method.

3.6.2 Order of kinetics (b)

The mechanism of recombination of de-trapped charge carriers with their counterparts is known as the order of kinetics (b). The order of kinetics can be predicted from shape of glow curve by using symmetry factor or geometric factor (μ_g) stated by Chen can be given as

$$\mu_g = \delta/\omega = T_2 - T_m/T_2 - T_1 \qquad (1)$$

The symmetry factor is to differentiate between first and second order TL glow peak. (μ_g) = 0.39–0.42 for the first order kinetics; (μ_g) = 0.49–0.52 for the second order kinetics and (μ_g) = 0.43–0.48 for the mixed order of kinetics [34].

3.6.3 Activation energy (E)

The knowledge about trapping parameters for calculating trap information in traps centre such as required energy for escaping one electron from trap centre known as activation energy or trap depth "E". So, the trap depth calculated by different methods proposed by several authors [35]. Trap depth for second order kinetics is calculated using the Eq. (2)

$$E = 2kT_m\left(1.76\frac{T_m}{\omega} - 1\right) \qquad (2)$$

where, k is Boltzmann constant, E is activation energy, T_m is temperature of peak position.

3.6.4 Frequency factor (s)

Frequency factor reflects the probability to escape of electrons from the traps after exposure of ionizing radiation and it is one of the important parameter of the phosphor characterization. Once the order of kinetics and activation energy were determined, the frequency factor (s) can be calculated from the Eq. (3)

$$\frac{\beta E}{kT_m^2} = s\left[1 + (b-1)\frac{2kT_m}{E}\right]\exp(E/KT_m) \qquad (3)$$

where b is order of kinetics, and β is the heating rate. In the present work $\beta = 5\,°Cs^{-1}$.

The calculated kinetic parameters of SrCaMgSi$_2$O$_7$:Eu^{3+} phosphor by the peak shape method was given in Table 2. In our case, the value of shape factor (μ_g) is 0.47, which indicates that it is a case of mixed (intermediate) order kinetics, approaching towards second order, responsible for deeper trap depth [36].

3.7 Photoluminescence (PL)

The emission spectrum of SrCaMgSi$_2$O$_7$:Eu^{3+} phosphor was excited at 396 nm was shown in Fig. 8. It can be seen that its emission spectra are all composed of several sharp lines from the characteristic Eu^{3+} emission. The excitation spectrum of SrCaMgSi$_2$O$_7$:Eu^{3+} phosphor exhibit a broad band in the UV region centered at about 255 nm, and several sharp lines between 300 and 400 nm. Eu^{3+} ions has a $4f^6$ configuration, it needs to gain one more electron to achieve the half-filled $4f^7$ configuration, which is relatively stable compared to partially filled configurations [37–39]. When Eu^{3+} is linked to the O ligand, there is a chance of electron transfer from O to Eu^{3+} to form Eu^{2+}–O^2 (simply Eu–O). During this, there is a broad absorption band at 240–270 nm, depending on the host. This is known as the Eu–O charge transfer band (CTB). It can be seen from Fig. 8, the excitation spectrum is composed of two major
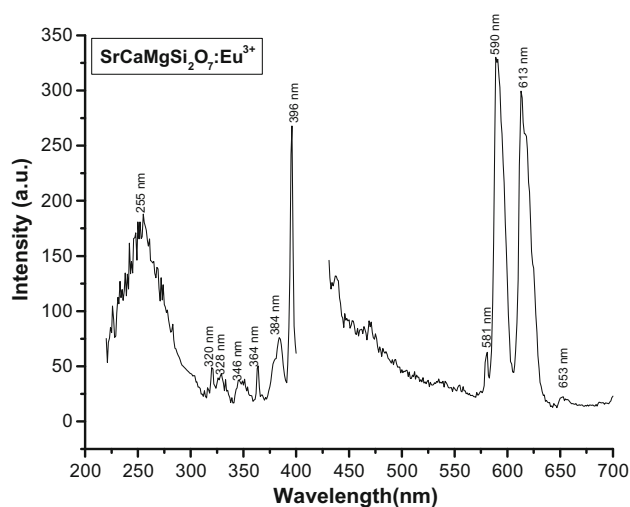
Fig. 8 Excitation and emission spectra of SrCaMgSi$_2$O$_7$:Eu^{3+} phosphor

parts: (1) the broad band between 220 and 300 nm, the broad absorption band is called charge transfer state (CTS) band due to the europium-oxygen interactions, which is caused by an electron transfer from an oxygen 2p orbital to an empty 4f shell of europium and the strongest excitation peak at about 255 nm. (2) A series of sharp lines between 300 and 400 nm, ascribed to the f–f transition of Eu^{3+} ions. The strongest sharp peak is located at 396 nm corresponding to $^7F_0 \rightarrow {}^5L_6$ transition of Eu^{3+}. Other weak excitation peaks are located at 320, 328, 346, 364 and 384 nm are related to the intra-configurational 4f–4f transitions of Eu^{3+} ions in the host lattices [40]. The prepared SrCaMgSi$_2$O$_7$:Eu^{3+} phosphor can be excited by near UV (NUV) at about 396 nm effectively. So, it can match well with UV and NUV-LED, showing a great potential for practical applications [41].

The emission spectra of SrCaMgSi$_2$O$_7$:Eu^{3+} phosphor was shown in Fig. 8 in the range of 400–700 nm. Under the 396 nm excitation, the emission spectrum of our obtained samples was composed of a series of sharp emission lines, corresponding to transitions from the excited states $^5D_0$ to the ground state ^7F_j (j = 0, 1, 2, 3) [42]. The orange emission at about 590 nm belongs to the magnetic dipole $^5D_0 \rightarrow {}^7F_1$ transition of Eu^{3+}, and the transition hardly varies with the crystal field strength. The red emission at 613 nm ascribes to the electric dipole $^5D_0 \rightarrow {}^7F_2$ transition of Eu^{3+} ions, which is very sensitive to the local environment around the Eu^{3+}, and depends on the symmetry of the crystal field. It is found that the 590 and 613 nm emissions are the two strongest peaks, indicating that there are two Sr^{2+} sites in the SrCaMgSi$_2$O$_7$:Eu^{3+} lattice [43]. One site, Sr (I), is inversion symmetry and the other site, Sr (II), is non-inversion symmetry. When doped in SrCaMgSi$_2$O$_7$:Eu^{3+} ions occupied the two different sites of
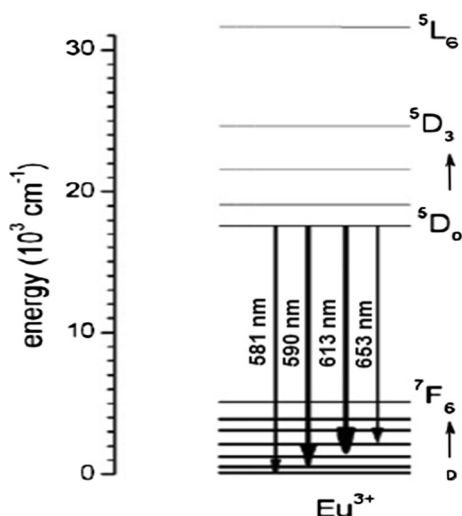
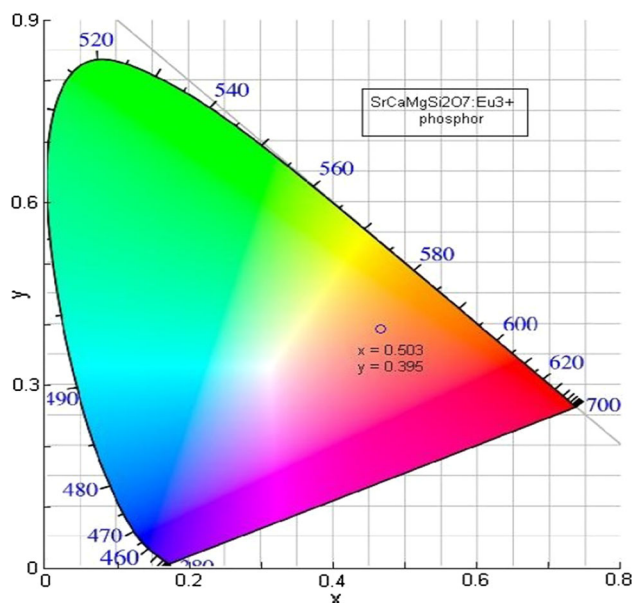**Fig. 9** Schematic energy level diagram of SrCaMgSi$_2$O$_7$:Eu^{3+} phosphor

Fig. 10 CIE chromaticity diagram of SrCaMgSi$_2$O$_7$:Eu^{3+} phosphor

Sr (I) and Sr (II). Other two emission peaks located at 581 and 653 nm are relatively weak, corresponding to the $^5D_0 \rightarrow ^7F_0$ and $^5D_0 \rightarrow ^7F_3$ typical transitions of Eu^{3+} ions respectively. The strongest emission is associated to the Eu^{3+} electric-dipole transition of $^5D_0$–$^7F_1$, and which implies that the Eu^{3+} occupies a center of inversion asymmetry in the host lattice. For the phosphor SrCaMgSi$_2$O$_7$:Eu^{3+} prepared in our experiment, the strongest orange emission peak is located at 590 nm will be dominated. It can be presumed that Eu^{3+} ions mainly occupy with an inversion symmetric center in host lattice [44]. Figure 9 shows the schematic energy level diagram of Eu^{3+} ions in the SrCaMgSi$_2$O$_7$ host depicting different emissions bands.

3.8 CIE chromaticity coordinate

In general, color of any phosphor material is represented by means of color coordinates. The luminescence color of the samples excited under 396 nm has been characterized by the CIE 1931 chromaticity diagram [45]. The emission spectrum of the SrCaMgSi$_2$O$_7$:Eu^{3+} phosphor was converted to the CIE 1931 chromaticity using the photoluminescent data and the interactive CIE software (CIE coordinate calculator) diagram as shown in Fig. 10.

Every natural color can be identified by (x, y) coordinates that are disposed inside the 'chromatic shoe' representing the saturated colors. Luminescence colors of Eu^{3+} doped SrCaMgSi$_2$O$_7$ phosphor are placed in the orange–red (x = 0.503, y = 0.395), corners. The chromatic co-ordinates of the luminescence of this phosphor are measure and reached to orange–red luminescence.

3.9 Decay

Figure 11 shows the typical decay curves of SrCaMgSi$_2$O$_7$:Eu^{3+} phosphor. The initial afterglow intensity of the sample was high. The decay times of phosphor can be calculated by a curve fitting technique, and the decay curves fitted by the sum of two exponential components have different decay times.

$$I = A_1 exp(-t/\tau_1) + A_2 exp(-t/\tau_2) \qquad (4)$$

where, I is phosphorescence intensity, A_1, A_2 are constants, t is time, τ_1 and τ_2 are decay times (in milisecond) for the exponential components. Decay curves are successfully fitted by the Eq. (4) [46] and the fitting curve result are shown in Table 3. The results indicated that the, afterglow decay curves are composed of two regimes, i.e., the initial rapid decaying process and the subsequent slow decaying process (Table 4).

As it was reported, when Eu^{3+} ions were doped into SrCaMgSi$_2$O$_7$, they would substitute the Sr^{2+} ions. To keep electro-neutrality of the compound, two Eu^{3+} ions would substitute three Sr^{2+} ions. The process can be expressed as Eq. (5)

$$2Eu^{3+} + 3Sr^{2+} \rightarrow 2[Eu_{Sr}]^* + [V_{Sr}]'' \qquad (5)$$

Each substitution of two Eu^{3+} ions would create two positive defects of [Eu$_{Sr}$]* capturing electrons and one negative vacancy of [V$_{Sr}$]''. These defects act as trapping centers for charge carriers. Then the vacancy [V$_{Sr}$]'' would act as a donor of electrons while the two [Eu$_{Sr}$]* defects become acceptors of electrons. By thermal stimulation, electrons of the [V$_{Sr}$]'' vacancies would then transfer to the
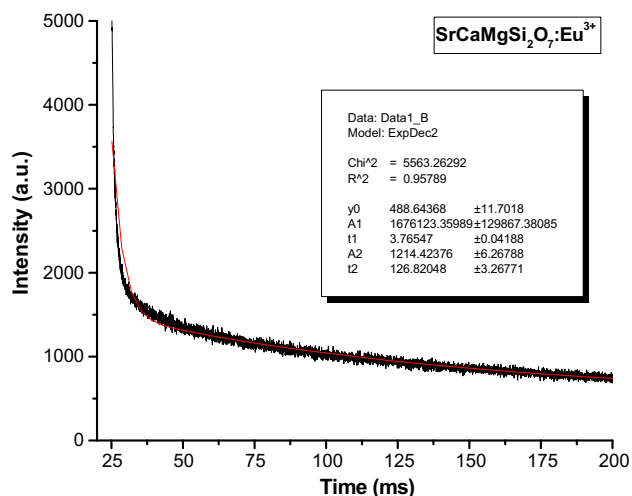
Fig. 11 Decay curves of $SrCaMgSi_2O_7:Eu^{3+}$ phosphor

Table 3 Fitting results of the decay curves

Phosphor	τ_1 (ms)	τ_2 (ms)
$SrCaMgSi_2O_7:Eu^{3+}$	3.76	126.82

Table 4 Calculation of ML decay constant

Impact velocity	10 cm	20 cm	30 cm	40 cm	50 cm
τ Decay constant (ms)	1.47	1.01	0.90	0.81	0.85

Eu^{3+} sites. The results indicate that the depth of the trap is too shallow leading to a quick escape of charge carriers from the traps resulting in a fast recombination rate in milliseconds (ms) [47].

3.10 Mechanoluminecsnce (ML)

ML also known as Triboluminescence was an important physical phenomenon where an emission of light was observed due to mechanical deformation of materials, when they are subjected to some mechanical stress like rubbing, cleavage, compressing, impulsive deformation, crushing, grinding, shaking etc. [48]. This phenomenon has been observed in many kinds of solids including ionic crystals, semiconductors, metals, glasses and organic crystals. In the present ML studies, an impulsive deformation technique has been used to deform the sintered phosphor. During the deformation of a solid, a great number of physical processes may occur within very short time intervals, which may excite or stimulate the process of photon emission. It is seen that when moving piston was released at particular height, then the ML emission also takes place [49, 50].

When the load was applied to the phosphor, initially the ML intensity increases with time, attains a peak value and then decreases with time. Such a curve between the ML intensity and deformation time of phosphors, was known as the ML glow curve. The prepared phosphor was fracture without any pre-irradiation such as X-ray, β-rays, γ-rays, UV, etc. Every time for the ML measurement, the quantity of $SrCaMgSi_2O_7:Eu^{3+}$ phosphor was kept constant (8 mg) and it was placed onto the upper surface of a transparent lucite plate which was kept inside the sample holder below the guiding cylinder. Then, it was covered with a thin aluminium foil and fixed using an adhesive tape [51]. This arrangement prevents the scattering of crystallite fragments during the impact of the load or piston on to the sample. The ML was excited impulsively by dropping a load onto the sample from different heights (h = 10, 20, 30, 40, 50 cm). The phosphor was fracture via dropping a load [moving piston] of particular mass (400 g) and cylindrical shape on the $SrCaMgSi_2O_7:Eu^{3+}$ phosphor. The velocity of the moving piston, holding the impact mass, could be changed (from 140 to 313 cm/s), by changing the height through which it was dropped. Figure 12 shows that the characteristics glow ML curve between ML intensity versus time for different heights. When the moving piston is dropped onto the prepared phosphor at different height, light is emitted. The photon emission time is nearly 2 ms, when prepared $SrCaMgSi_2O_7:Eu^{3+}$ phosphor fractures. In these ML measurements, maximum ML intensity has been obtained for the 50 cm dropping height and ML intensity increases with the falling height of the moving piston. [52].

Figure 12 (Inset) shows that the characteristics curve between ML intensity versus impact velocity of $SrCaMgSi_2O_7:Eu^{3+}$ phosphor. The ML intensity increases linearly with the increases the falling height of the moving piston; that is, the ML intensity depends upon the impact velocity of the moving piton [$v_0 = \sqrt{2gh}$ (where "**g**" is the acceleration due to gravity and "**h**" is the height through which the load is dropped freely)]. The ML intensity of $SrCaMgSi_2O_7:Eu^{3+}$ phosphor increases linearly with increasing the mechanical stress [53].

When the load or piston makes an impact on the crystal with an initial velocity v_0, the former decelerates and after a particular time its velocity becomes zero. The time dependence of the velocity of the piston may be written as
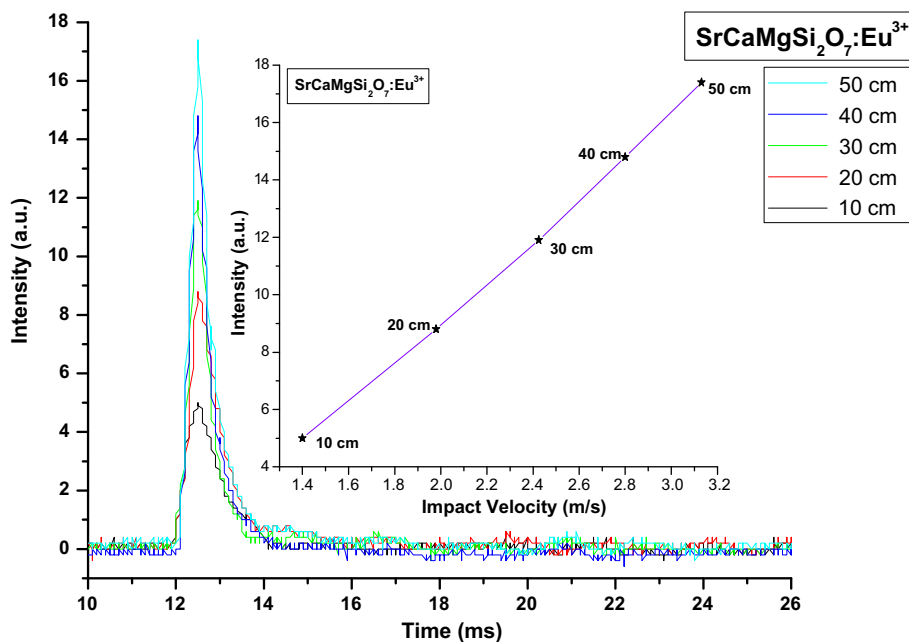
$$v = v_0 \exp(-\beta v_o t) \qquad (6)$$

where β is a constant, Eq. (6) can be written as

$$\frac{dx}{dt} = v_0 \exp(-\beta v_o t) \qquad (7)$$

where dx is the compression of the crystal during the time interval dt. Integrating Eq. (7), we have

Fig. 12 ML intensity versus time curve of SrCaMgSi$_2$O$_7$:Eu^{3+} phosphor (Inset—ML intensity versus impact velocity curve of SrCaMgSi$_2$O$_7$:Eu^{3+} phosphor)

$$x = \frac{1}{\beta}\exp(-\beta v_o t) + C \tag{8}$$

x = 0 for t = 0, therefore, Eq. (8) may be written as

$$x = \frac{1}{\beta}[1 - \exp(-\beta v_o t)] \tag{9}$$

The prepared phosphor is in powder form and the impact velocities compress it to a certain extent, but this does not change significantly with increasing impact velocity. Equation (9) shows that impact time remains mostly unchanged with increasing impact velocity because there is no significant change in compression, which is expressed by 'x' in Eq. (9). This may be one possible reason why the time that corresponds to the peak ML intensity does not change significantly with increasing impact velocity [54]. Figure 13 shows the time corresponds to ML signal peak with impact velocity of SrCaMgSi$_2$O$_7$:Eu^{3+} phosphor.

The relationship between semi-log plot of ML intensity versus (t–t$_m$) for SrCaMgSi$_2$O$_7$:Eu^{3+} phosphor is shown in Fig. 14, and the lines were fitted using the equation (10) with Origin Pro 8.0

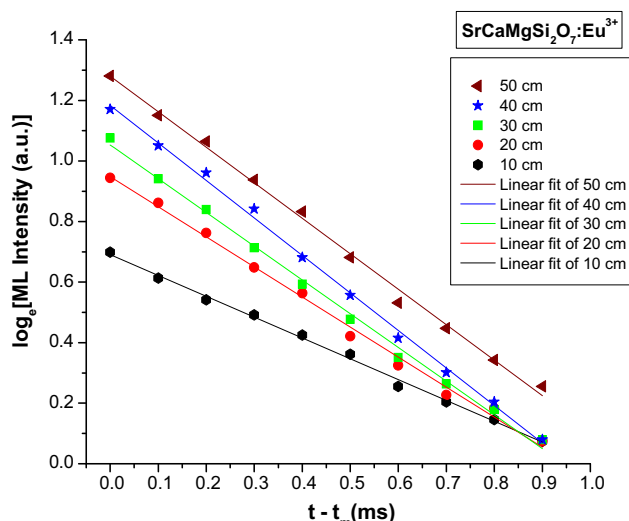$$\tau = \frac{1}{slop\,of\,straight\,line} \tag{10}$$

Curve fitting results show that decay constant (τ) varies from 1.47 to 0.85 ms. The ML decay constant value was decreases with the impact velocities, and maximum for the minimum impact velocities (See table 4). In order to further clarification of the ML decay mechanism in SrCaMgSi$_2$O$_7$:Eu^{3+} phosphor, more experimental and theoretical studies are needed.
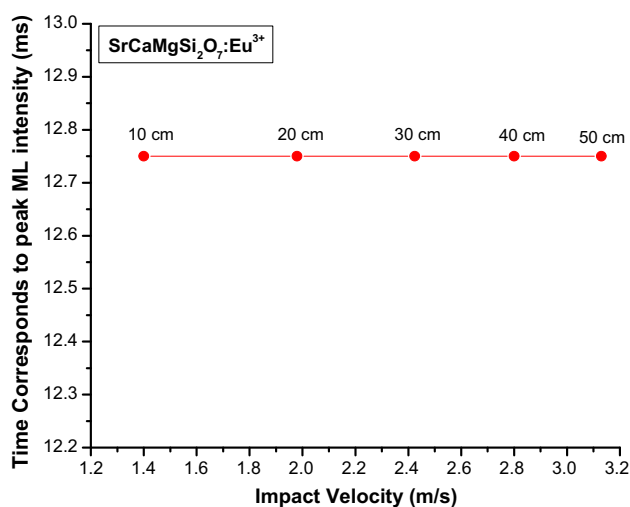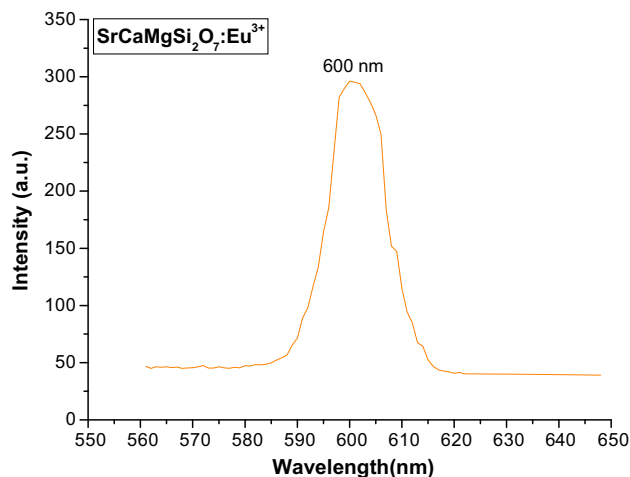

Fig. 13 Time corresponds to ML signal peak with impact velocity of SrCaMgSi$_2$O$_7$:Eu^{3+} phosphor

Figure 15 shows that the ML spectrum of SrCaMgSi$_2$O$_7$:Eu^{3+} phosphor. The peak location of the ML spectra (600 nm) and TL (600 nm) are similar, which suggests that the ML spectra also originates from the same emitting center of the Eu^{3+} ions, responsible for the orange–red ML emission.

When a mechanical stress, such as compress, friction, and striking, and so on, was applied on the sintered SrCaMgSi$_2$O$_7$:Eu^{3+} phosphors, piezo-electric field can be produced. Therefore, in such phosphor the ML excitation may be caused by the local piezoelectric field near the impurities and defects in the crystals. During the impact on
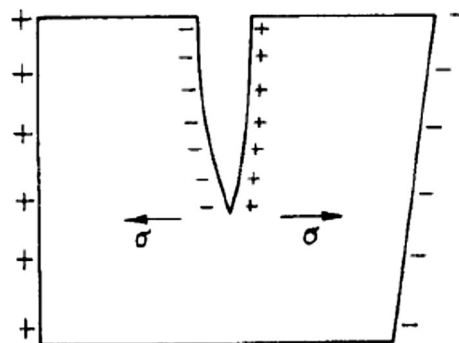
Fig. 14 Semi-log plot of ML intensity versus (t–t$_m$) for SrCaMgSi$_2$O$_7$:Eu^{3+} phosphor

Fig. 15 ML spectra of SrCaMgSi$_2$O$_7$:Eu^{3+} phosphor

Fig. 16 Langevin model for the piezo-electrification induce phosphor

increases with the increasing impact velocity. Thus, the ML intensity will increase proportionally with increasing value of impact velocity [56, 57].

As the impact velocity increases, the impact pressure also increases leading to the increase in the electric field at local region which causes the decrease in trap depth. Hence the probability of de-trapping increases. From Fig. 12 (inset), it can be seen that with increasing impact velocity, ML intensity also increases linearly i.e., the ML intensity of SrCaMgSi$_2$O$_7$:Eu^{3+} phosphors are linearly proportional to the magnitude of the impact velocity. When the surface of an object was coated with the ML materials, the stress distribution in the object beneath the layer could be reflected by the ML brightness and could be observed. Based on the above analysis these phosphors can also be used as sensors to detect the stress of an object [58].

4 Conclusion

A new orange–red emitting SrCaMgSi$_2$O$_7$:Eu^{3+} phosphor was synthesized by high temperature solid state reaction method at 1200 °C and its structural characterization and luminescence properties were investigated. The tetragonal structure of prepared phosphor was confirmed by the XRD. Photoluminescence measurements showed that the phosphor exhibited emission peak with good intensity at 590 and 613 nm, corresponding to $^5D_0 \rightarrow {}^7F_1$ orange emission and weak $^5D_0 \rightarrow {}^7F_2$ red emission. The excitation band at 396 nm can be assigned to $^7F_0 \rightarrow {}^5L_6$ transition of Eu^{3+} ions due to the typical f–f transitions. CIE color chromaticity diagram, TL spectra and ML spectra confirms SrCaMgSi$_2$O$_7$:Eu^{3+} phosphor exhibits orange–red emission and excellent color stability, indicating that it has favorable properties for application as near ultraviolet LED conversion phosphor. The phosphorescent life time of SrCaMgSi$_2$O$_7$:Eu^{3+} phosphor can be calculated by a curve fitting technique, and the decay curves fitted by the sum of two exponential components have different decay times

the material, one of its newly created surfaces gets positively charged and the other surface of the crack gets negatively charged (Fig. 16). Thus, an intense electric field in the order of 10^6–10^7 V cm^{-1} is produced [55]. Under such order of electric field, the ejected electrons from the negatively charged surface may be accelerated and subsequently their impact on the positively charged surfaces may excite the luminescence center. Thus, depending on the prevailing conditions, recombination luminescence may be produced. For the impact velocity, the impact pressure P$_0$ will be equals to, P$_0$ = Zυ$_0$, where Z is a constant. With increasing value of impact velocity, the trap depth will decrease, therefore, for the trap depth beyond a particular pressure the traps will be unstable and they will be de-trapped, in which the number of de-trapped electrons will

($\tau_1 = 3.76$ ms; $\tau_2 = 126.82$ ms) and they possess the fast and slow decay process. It is worthy to note that the dependence between ML intensity of $SrCaMgSi_2O_7:Eu^{3+}$ and the impact velocity of the moving piston is close to linearity, which suggests these phosphors can also be used as sensors to detect the stress of an object.

References

1. H.W. Leverenz, *An introduction to luminescence of solids* (Dover Publications Inc., New York, 1968)
2. I.P. Sahu, D.P. Bisen, N. Brahme, J. Biol. Chem. Lumin. (2014). doi:10.1002/bio.2869
3. J. Qing-Ze, T.Z. Ling, Z. Yun, J. Nanopart. Res. **9**, 519 (2003)
4. Z. Song, J. Liao, X. Ding, T. Zhou, Q.L. Liu, J. Lumin. **132**, 1768 (2012)
5. T.W. Kuo, T.M. Chen, Opt. Mater. **32**, 882 (2010)
6. X. Dong, J. Zhang, X. Zhang, Z. Hao, Y. Luo, J. Alloys Compd. **587**, 493 (2014)
7. C. Gorller-Walrand, L. Fluyt, A. Ceulemans, W.T. Carnall, J. Chem. Phys. **1991**, 3099 (1995)
8. I.P. Sahu, D.P. Bisen, N. Brahme, Res. Chem. Intermed. (2014). doi:10.1007/s11164-014-1767-6
9. I.P. Sahu, D.P. Bisen, N. Brahme, L. Wanjari, R.K. Tamrakar, Res. Chem. Intermed. **41**, 8797 (2015)
10. G. Talwar, C.P. Joshi, S.V. Moharil, S.M. Dhopte, P.L. Muthal, V.K. Kondawat, J. Lumin. **129**(11), 1239 (2009)
11. Z. Xiao, Z. Xiao, US Patent No. 6-093-346. (2000)
12. Y. Xu, D. Chen, Ceram. Int. **34**, 2117 (2008)
13. M. Xu, L. Wang, L. Liu, D. Jia, R. Sheng, J. Lumin. **146**, 475 (2014)
14. I.P. Sahu, J. Mater. Sci. Mater. Electron. (2015). doi:10.1007/s10854-015-3327-2
15. H. Zhang, N. Terasaki, H. Yamada, C.N. Xu, Key Eng. Mater. **388**, 305 (2009)
16. C.N. Xu, T. Watanabe, M. Akiyama, X.G. Zheng, Appl. Phys. Lett. **74**(17), 2414 (1999)
17. C.N. Xu, X.G. Zheng, M. Akiyama, K. Nonaka, T. Watanabe, Appl. Phys. Lett. **76**(2), 179 (2000)
18. JCPDS file number 75-1736, JCPDS International Center for Diffraction Data
19. JCPDS file number 77-1149, JCPDS International Center for Diffraction Data
20. I.P. Sahu, D.P. Bisen, R.K. Tamrakar, R. Shrivastava, Res. Chem. Intermed. (2015). doi:10.1007/s11164-015-2120-4
21. I.P. Sahu, D.P. Bisen, N. Brahme, R.K. Tamrakar, J. Lumin. **167**, 278 (2015)
22. H. Zhang, N. Terasaki, H. Yamada, C. N. Xu, Electrochem. Solid-State Lett. **10**(10), J129 (2007)
23. I.P. Sahu, D.P. Bisen, N. Brahme, Displays **35**, 279 (2014)
24. M.A. Salim, R. Hussain, M.S. Abdullah, S. Abdullah, N.S. Alias, Solid State Sci. Technol. **17**, 59 (2009)
25. Z. Gou, J. Chang, W. Zhai, J. Eur. Ceram. Soc. **25**, 1507 (2005)
26. I.P. Sahu, D.P. Bisen, N. Brahme. Displays **38**, 68 (2015)
27. Z. Zhang, Y. Wang, H. Wang, Z. Sun, L. Jia, J. Phys. Conf. Ser. **152**, 012050 (2009)
28. C. Chang, D. Mao, J. Alloys Compd. **390**, 133 (2005)
29. G.T. Chandrappa, S. Ghosh, K.C. Patil, J. Mater. Synth. Process. **7**, 273 (1999)
30. Z. Yuan, C. Chang, D. Mao, W.J. Ying, J. Alloys Compd. **377**(1–2), 268 (2004)
31. I.P. Sahu, D.P. Bisen, N. Brahme, R.K. Tamrakar, J. Mater. Sci. Mater. Electron. (2015). doi:10.1007/s10854-015-3691-y
32. R. Shrivastava, J. Kaur, Indian J. Phys. (2014). doi:10.1007/s12648-014-0535-1
33. H.B. Premkumar, H. Nagabhushana, S.C. Sharma, S.C. Prashantha, H.P. Nagaswarupa, B.M. Nagabhushana, R.P.S. Chakradhar, J. Alloys Compd. **601**, 75 (2014)
34. I.P. Sahu, D.P. Bisen, N. Brahme, M. Ganjir, Lumin. J. Biol. Chem. Lumin. (2015). doi:10.1002/bio.2900
35. V. Pagonis, G. Kitis, C. Furetta, *Numerical and practical exercises in thermoluminescence* (Springer, Berlin, 2006)
36. R. Chen, S.W.S. McKeever, *Theory of thermoluminescence and related phenomenon* (World Scientific Press, Singapore, 1997)
37. H. Wu, Y. Hu, Y. Wang, F. Kang, Z. Mou, Opt. Laser Technol. **43**, 1104 (2011)
38. I.P. Sahu, D.P. Bisen, N. Brahme, J. Radiat. Res. Appl. Sci. **8**, 381 (2015)
39. I.P. Sahu, D.P. Bisen, N. Brahme, R.K. Tamrakar, J. Radiat. Res. Appl. Sci. **8**, 104 (2015)
40. S.P. Kuang, K. Liang, J. Liu, Y.M. Mei, M. Jiang, Z.C. Wu, D.X. Li, Optik (2014). doi:10.1016/j.ijleo.2013.12.037
41. H.Y. Jiao, Y. Wang, Phys. B **407**, 2729 (2012)
42. H. Nagabhushana, D.V. Sunitha, S.C. Sharma, B. Daruka Prasad, B.M. Nagabhushana, R.P.S. Chakradhar, J. Alloys Compd. **595**, 192 (2014)
43. C. Devayani, S.K. Omanwar, S.V. Moharil, J. Lumin. **142**, 180 (2013)
44. G. Vicentinia, L.B. Zinner, J. Zukerman-Schpector, K. Zinner, Coord. Chem. Rev. **196**, 353 (2000)
45. CIE, International Commission on Illumination. Publication CIE no. 15 (E-1.3.1). (1931)
46. R. Shrivastava, J. Kaur, Chin. Chem. Lett. (2015). doi:10.1016/j.cclet.2015.05.028
47. T. Aitasalo, P. Daren, J. Holsa, K. Junger, J.C. Krupa, M. Lastusaari, J. Legendziewicz, J. Niittykoski, W. Strek, J. Solid State Chem. **171**, 114 (2003)
48. D.R. Vij, *Luminescence of solids* (Plenum Press, New York, 1998)
49. I.P. Sahu, D.P. Bisen, N. Brahme, R.K. Tamrakar, J. Mater. Sci. Mater. Electron. **26**, 8824 (2015)
50. B.P. Chandra, J. Lumin. **131**, 1203 (2011)
51. I.P. Sahu, D.P. Bisen, N. Brahme, Lumin. J. Biol. Chem. Lumin. **30**(5), 526 (2015)
52. I.P. Sahu, P. Chandrakar, R.N. Baghel, D.P. Bisen, N. Brahme, R.K. Tamrakar, J. Alloys Compd. **649**, 1329 (2015)
53. B.P. Chandra, A.S. Rathore, Cryst. Res. Technol. **30**, 885 (1995)
54. H. Zhang, N. Terasaki, H. Yamada, C.N. Xu, Thin Solid Films **518**, 610 (2009)
55. I.P. Sahu, D.P. Bisen, R.K. Tamrakar, R.K. Tamrakar, R. Shrivastava, J. Mater. Sci. Mater. Electron. (2015). doi:10.1007/s10854-015-3667-y
56. H. Zhang, N. Terasaki, H. Yamada, C.N. Xu, Int. J. Modern Phys. B **23**, 1028 (2009)
57. I.P. Sahu, D.P. Bisen, R. Sharma, Res. Chem. Intermed. (2015). doi:10.1007/s11164-015-2177-0
58. H. Zhang, C.N. Xu, N. Terasaki, H. Yamada, Phys. E **42**, 2872 (2010)